SNAP TELESCOPE

M. Sholl[1], M. Lampton[1], G.Aldering[2], W. Althouse[3], R. Amanullah[4], J. Annis[5], P. Astier[6], C. Baltay[7], E. Barrelet[6], S. Basa[8], C. Bebek[2], L. Bergström[4], G. Bernstein[9], M. Bester[1], B. Bigelow[10], R. Blandford[3], R. Bohlin[11], A. Bonissent[12], C. Bower[13], M. Brown[10], M. Campbell[10], W. Carithers[2], E. Commins[1], W. Craig[3], C. Day[2], F. DeJongh[5], S. Deustua[14], T. Diehl[5], S. Dodelson[5], A. Ealet[8], R. Ellis[15], W. Emmet[7], D. Fouchez[12], J. Frieman[5], A. Fruchter[11], D. Gerdes[10], L. Gladney[9], G. Goldhaber[1], A. Goobar[4], D. Groom[2], H. Heetderks[1], M. Hoff[2], S. Holland[2], M. Huffer[3], L. Hui[5], D. Huterer[16], B. Jain[9], P. Jelinsky[1], A. Karcher[2], S. Kahn[3], S. Kent[5], A. Kim[2], W. Kolbe[2], B. Krieger[2], G. Kushner[2], N. Kuznetsova[2], R. Lafever[2], J. Lamoureux[2], O. Le Fèvre[8], M. Levi[2], P. Limon[5], H. Lin[5], E. Linder[2], S. Loken[2], W. Lorenzon[10], R. Malina[8], J. Marriner[5], P. Marshall[3], R. Massey[17], A. Mazure[8], T. McKay[10], S. McKee[10], R. Miquel[2], N. Morgan[7], E. Mörtsell[4], N. Mostek[13], S. Mufson[13], J. Musser[13], P. Nugent[2], H. Oluşeyi[2], R. Pain[6], N. Palaio[2], D. Pankow[9], J. Peoples[5], S. Perlmutter[2], E. Prieto[8], D. Rabinowitz[7], A. Refregier[18], J. Rhodes[15], N. Roe[2], D. Rusin[9], V. Scarpine[5], M. Schubnell[10], G. Smadja[19], R. M. Smith[15], G. Smoot[1], J. Snyder[7], A. Spadafora[2], A. Stebbins[5], C. Stoughton[5], A. Szymkowiak[7], G. Tarlé[10], K. Taylor[15], A. Tilquin[12], A. Tomasch[10], D. Tucker[5], D. Vincent[6], H. von der Lippe[2], J-P. Walder[2], G. Wang[2], W. Wester[5]

[1]University of California at Berkeley
[2]Lawrence Berkeley National Laboratory
[3]Stanford Linear Accelerator Center
[4]University of Stockholm
[5]Fermi National Accelerator Laboratory
[6]LPNHE, CNRS-IN2P3, Paris, France
[7]Yale University
[8]LAM, CNRS-INSU, Marseille, France
[9]University of Pennsylvania
[10]University of Michigan
[11]Space Telescope Science Institute
[12]CPPM, CNRS-IN2P3, Marseille, France
[13]Indiana University
[14]American Astronomical Society
[15]California Institute of Technology
[16]Case Western Reserve University
[17]Cambridge University
[18]CEA, Saclay, France
[19]IPNL, CNRS-IN2P3, Villeurbanne, France

ABSTRACT

Mission requirements, the baseline design, and optical systems budgets for the SuperNova/Acceleration Probe (SNAP) telescope are presented. SNAP is a proposed space-based experiment designed to study dark energy and alternate explanations of the acceleration of the universe's expansion by performing a series of complementary systematics-controlled astrophysical measurements. The goals of the mission are a Type Ia supernova Hubble diagram and a wide-field weak gravitational lensing survey. A 2m widefield three-mirror telescope feeds a focal plane consisting of 36 CCDs and 36 HgCdTe detectors and a high-efficiency, low resolution integral field spectrograph. Details of the

Optical, Infrared, and Millimeter Space Telescopes, edited by John C. Mather,
Proceedings of SPIE Vol. 5487 (SPIE, Bellingham, WA, 2004)
0277-786X/04/$15 · doi: 10.1117/12.552081

maturing optical system, with emphasis on structural stability during terrestrial testing as well as expected environments during operations at L2 are discussed. The overall stray light mitigation system, including illuminated surfaces and visible objects are also presented.

Keywords: three-mirror telescopes, space astronomy, dark energy, wide-field imaging
Contact: sholl@ssl.berkeley.edu

1. SNAP MISSION OVERVIEW

The SNAP (SuperNova/Acceleration Probe, see Figures 1 and 2) is a planned space-based experiment designed to study dark energy and test alternate explanations for the expansion history of the universe[1]. The experiment is motivated by a recent discovery that the expansion rate of the universe is increasing.[2,3] This observation suggests that the universe contains a form of dark energy which can be modeled by its equation of state at the present epoch w_0, and its rate of change with redshift w'.

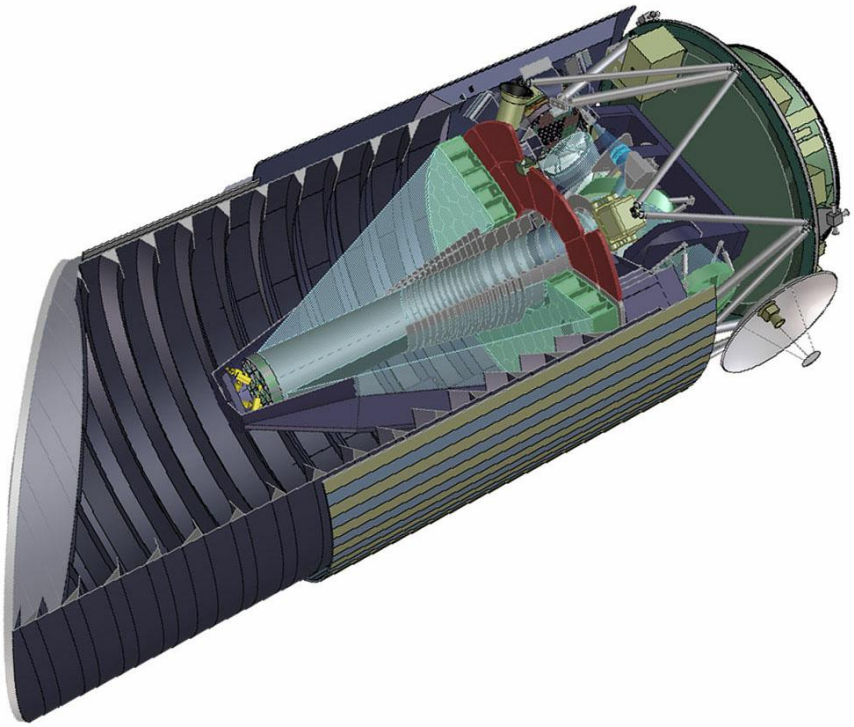

Figure 1: SNAP Observatory

Type Ia supernovae populate the observable universe, and are sufficiently consistent in magnitude and spectral characteristics to allow their use as standard candles. By measuring the irradiance of a supernova at peak, one may discern the distance to the supernova when the radiation was emitted, and hence the elapsed time since the supernova event. The redshift provides a measure of the expansion rate of the universe during the supernova's epoch. Properly calibrated and sorted into systematic classes, a collection of a few thousand such supernovae spanning the redshift range $0.1<z<1.7$ will provide important new constraints on models of the universe and the dark energy suggested by the observation of universal acceleration.

A widefield survey covering 1000 square degrees resolves ~100 galaxies per square arcminute (300 million galaxies total). The SNAP observatory produces a stable point spread function over a wide field of view, therefore independent constraints on the evolution of the universe can be obtained from the observation of weak gravitational lensing of background galaxies by foreground mass concentrations.

The SNAP observatory is built around an advanced three-mirror anastigmat telescope, and will perform mission operations at the L2 Lagrange point. Details of the mission, science background, and the scientific goals of the campaign are presented at http://snap.lbl.gov (the SNAP home page) and elsewhere in the literature.[4,5,6] The SNAP telescope design and status was summarized in earlier works by Lampton et al.[7,8,9] Design of the SNAP telescope matured substantially since these works were published, and progress on the telescope design as well as a review of the optical configuration are the primary focus of this paper.

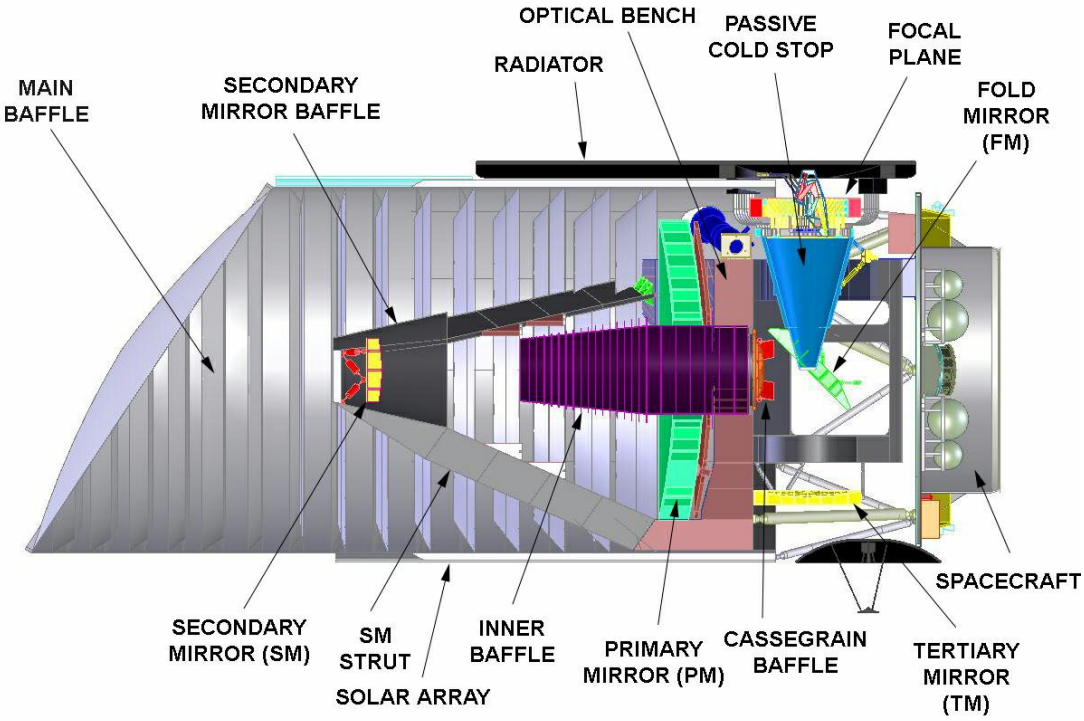

Figure 2: SNAP Observatory cross section. The observatory structural center is the disk-shaped spacecraft located toward the right of the figure. The optical bench is mounted to the spacecraft via semi-kinematic bipod mounts, and the main optical baffle (center-left baffled cylinder) also mounts to the spacecraft via six bipods. A monolithic front cover is ejected subsequent to observatory arrival at L2. A solar array (lower) provides power to the observatory, and a radiator (upper right) provides passive cooling for the 140K focal plane array.

2. BASELINE MISSION

In order to determine the optimal sky survey area, field of view, wavelength coverage and observing plan, we have conducted detailed simulations of a variety of payload designs and mission scenarios and judged them according to their science return. Our current baseline specifies a telescope aperture of 2.0 meters, an effective focal length of 21.66 meters (plate scale = 105 microns/arcsecond) and a wavelength range of 0.35 to 1.7 microns in nine photometric bands. The focal plane is an annular mosaic[10] of 36 large-format NIR detectors (18 um pixels, three filter bands) and 36 large format silicon visible detectors (10.5 um pixels, six filter bands). Dithering in a 2x2 pattern allows each exposure to be sampled appropriately. The focal plane assembly includes a spectrograph[11] with which supernova spectra will be measured within a few days of peak irradiance for classification.

For the supernova work, a 7.5 square degree region near the north ecliptic pole will be scanned repeatedly on a 4 day cadence for approximately 16 months. Each scan delivers nine-band photometry on everything in this field. Within each 4-day period, 1-2 days are used for targeted spectroscopy of supernovae. Later in the mission, a 7.5 square degree region near the south ecliptic pole will be surveyed similarly. It is expected that several thousand supernovae in the redshift range 0.35-1.7 will have accurate redshifts and magnitudes determined by these surveys.

For the weak lensing work, a much larger field (~1000 square degrees) will be surveyed once, using approximately 10 months of the mission. Because these surveys are lengthy, the motion of the sun along the ecliptic must be accommodated. Our payload is baffled against sunlight on one side where the primary solar power array is located. Every 90 days, we plan to conduct a 90 degree roll maneuver to maintain solar array orientation toward the mean sun. Accordingly our focal plane has 90 degree roll symmetry so that survey work need not be interrupted.

An orbit location at the Earth-Sun L2 position[12] avoids radiation belt passages and provides a highly stable thermal environment. Also advantageous is its freedom from stray light from the full Earth, which can be a serious problem from LEO or HEO.

3. OPTICAL DESIGN

SNAP mission requirements call for a wide-field telescope with diffraction limited performance over the 0.35-1.7μm band. In order to match the desired plate scale (0.1arcsec/pixel) to the pixel size of the CCD detectors (10.5μm), a telescope focal length of ~22m is necessary. A 22m focal length Paul-Baker, Cassegrain, or Ritchey-Chretien telescope is difficult to integrate within a typical launch vehicle fairing. A three-mirror anastigmat (TMA) configuration, developed by Korsch[13], may deliver a large focal length telescope in a package with a physical to focal length ratio (telephoto advantage) of 1/7. Such a compact telescope (see Figure 3) is compatible with typical fairings. An added benefit of this design is location of the focal plane near the outer envelope of the telescope. This allows the focal plane to be placed near a radiator for passive cooling to 140K.

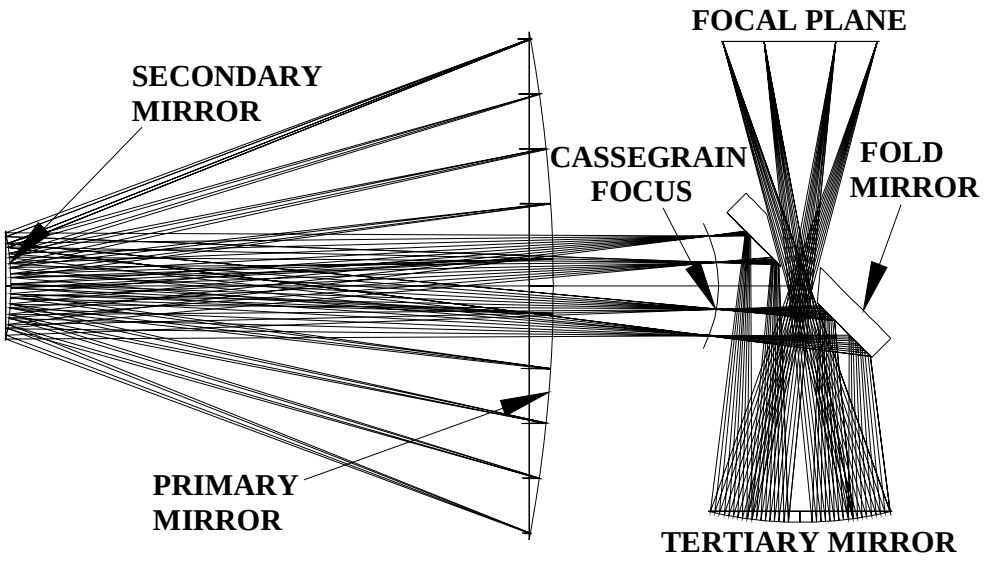

Figure 3: SNAP Optics Layout. The system entrance pupil is defined by the active perimeter of the primary mirror (PM). An image of the pupil is located near the hole in the fold mirror (FM). A field stop is located at the Cassegrain focus.

A baseline optical prescription was developed using a non-linear least squares method.[14] The general strategy involved defining mirror separations primary-secondary, secondary-tertiary and tertiary-focal plane for packaging into the fairing, and allowing an optimization routine to adjust curvature and conic constants of the three curved mirrors. The entrance aperture, focal plane diameter and focal length were considered as given. Secondary-tertiary and tertiary-focal plane spacing were adjusted iteratively to preclude vignetting at the fold mirror, and the design re-optimized until a satisfactory configuration was achieved. The design consists of a concave ellipsoidal primary and tertiary mirrors, and a convex hyperbolic secondary. Full details of the design, along with spot diagrams and additional diagnostics are reported in Lampton et al.[7,8,9]

4. SYSTEM BUDGETS

The RMS geometric blur reported by Lampton (2.8μm average, one dimension) corresponds to a point spread function (PSF) produced by an undistorted, contamination-free telescope. Real-world effects such as misalignment, figure errors introduced by structural flexibility, polishing errors, thermal distortion, and 1-g release are tracked in an optical path difference (OPD) system budget. For small OPD errors, the Marechal approximation facilitates conversion of wavefront errors (WFE) to a focal-plane Strehl.[15] The image quality requirement of the telescope is driven in part by the SNR requirement, and also by the potential systematic supernova spectrum contamination by unwanted light from the supernova host galaxy. The present baselined Strehl requirement is 0.90 at 1μm. This corresponds to an RMS wavefront error (WFE) of 51nm, and a Strehl of 0.77 at the common helium neon (0.633μm).wavelength

The telescope is expected to be aligned via standard surveying techniques. Five degree of freedom motion of the secondary mirror (mounted on a 100nm precision hexapod) will be commanded to final alignment during ground-based interferometric testing. On orbit, starfield PSF data will be used to correct launch-induced and long-term changes to the optical alignment. This alignment strategy complicates mechanical tolerancing, because the ability of the secondary mirror to reduce RMS geometric blur to a certain degree must be included in the mechanical tolerancing/WFE budgeting exercise. A simulated on-orbit PSF minimization algorithm was implemented within an optical raytrace observatory simulation to determine correctible mechanical tolerance levels for the telescope. This study showed that initial alignment tolerances are within the capability of surveying equipment, and that the corrected spot size meets requirements for the mission.[16] Table 1 details the post-correction WFE budget, and Table 2 shows initial alignment tolerances for the observatory and performance levels achieved after system re-optimization via motion of the SM hexapod.

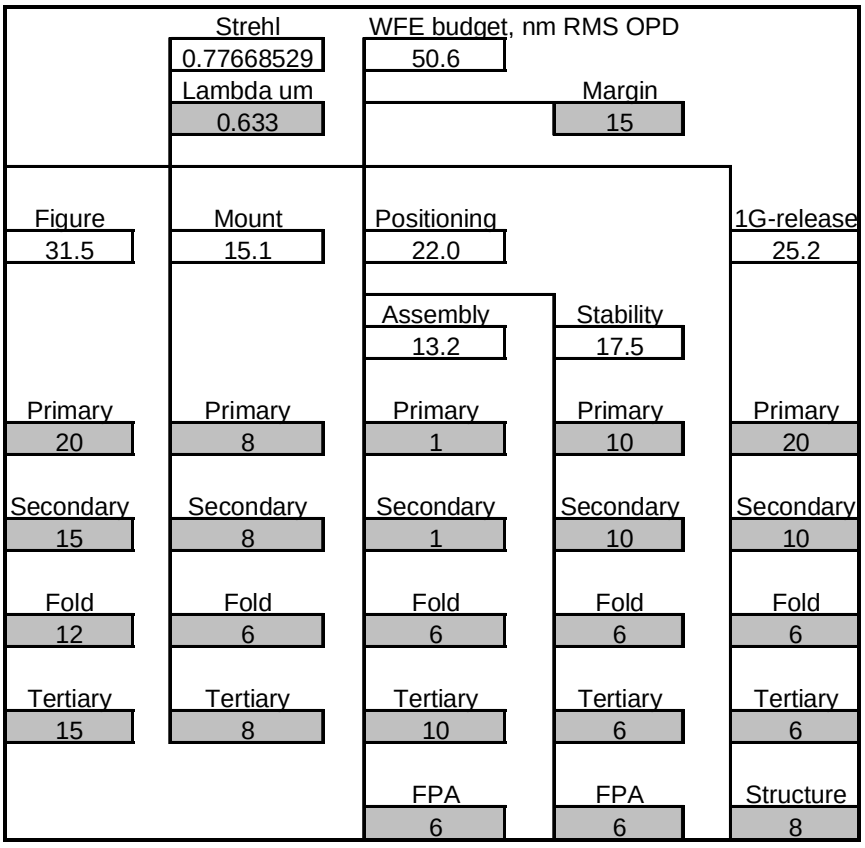

TABLE 1: Wavefront error (WFE) budget. Listed are pupil-plane optical path differences (nm RMS OPD) for the various optical elements, construction and operational phases.

Misalignment	Axis	Magnitude	WFE after SM correction (nm)	WFE sum (nm)	WFE budget (nm)
Secondary position	X	500µm	0.0	0.9	1.0
	Y	500µm	0.0		
	Z	100µm	0.0		
Hexapod linear errors		100nm	0.9		
Secondary rotation	X	500µrad	0.0		
	Y	500µrad	0.0		
Hexapod rotary errors		0.5µrad	0.1		
Fold position	X	100µm	3.8	5.4	6.0
	Y	500µm	0.0		
	Z	100µm	2.6		
Fold rotation	X	100µrad	2.1		
	Y	50µrad	2.0		
	Z	500µrad	0.0		
Tertiary position	X	500µm	4.5	7.7	10.0
	Y	100µm	4.0		
	Z	100µm	3.4		
Tertiary rotation	X	50µrad	2.4		
	Y	50µrad	2.4		
Focal plane pos	X	500µm	0.0	4.4	6.0
	Y	500µm	0.0		
	Z (focal plane)	100µm	0.1		
	Z (chip to chip)	25µm	4.0		
Focal plane rotation	X	500µrad	0.0		
	Y	100µrad	1.2		
	Z	100µrad	1.2		

TABLE 2: Initial alignment tolerances, and optical performance after correction via motion of the SM

Due to the non-zero coefficient of thermal expansion (CTE) of materials from which the telescope, structure and instruments are made, thermal gradients and bulk temperature changes can change the shape of the telescope elements.[17] In an optimal telescope design such as TMA63, this generally leads to degradation of the PSF. Because the weak lensing mission demands PSF stability, short-term stability levels of the telescope stem primarily from weak lensing requirements, not overall Strehl. Short-term excursion and stability requirements, therefore, are tracked separately from those thermal effects and misalignments which may be corrected by infrequent optimization using motion of the secondary mirror. Precise active thermal control will be necessary on the primary mirror (PM), secondary mirror (SM), and SM support struts, and to a lesser degree on the fold mirror (FM), tertiary mirror (TM) and focal plane (FP).

	Material CTE (ppb/K)	Thermal control requirement, ±ºC		
		Primary	Secondary	Tertiary
ULE™ Premium grade	10	10.2	90.9	357.1
ULE™ Mirror grade	15	6.80	60.6	238.1
Zerodur™ (class 0)	20	5.10	45.5	178.6
Zerodur™ (class 1)	50	2.04	18.2	71.4
Zerodur™ (class 2)	100	1.02	9.09	35.7
Silicon Carbide	2770	0.037	0.33	1.29
Beryllium	11400	0.0090	0.08	0.31
Mirror radius of curavature	Specification (m)	4.90	1.10	1.40
	Tolerance (µm)	0.50	1.00	5.00

TABLE 3: Thermal control requirements for TMA-63 mirrors constructed of typical substrate materials are listed. Mirrors temperatures must be controlled to these levels in order to keep mirror radii of curvatures within the tolerances listed at the bottom of the table. Control requirements $\leq \pm 1$ºC are considered difficult. The worst-case situation of uncorrelated temperature excursions is assumed.

As shown in Table 3, bulk radius of curvature changes caused by thermal excursions of the PM and SM suggest ULE™ and Zerodur™ do not present difficult thermal control challenges, while SiC substrates require more precise

thermal control. The TM temperature stability requirements are easily met by ULE™ or Zerodur™, and somewhat challenging for SiC. Not listed in the table is the flat fold mirror. Through-the-thickness gradients are the main possible source of thermal errors on the FM. The ratio of CTE to thermal conductivity is similar for ULE™, Zerodur™ and SiC (see Table 5), and all three materials are thermo-mechanically compatible with the FM design. Requirements of 1-g testing, as will be seen in the next section, drive material selection for the FM. It is interesting to note that a structure fabricated entirely from a moderate CTE material such as SiC retains imaging properties when the bulk temperature is changed. Such a gradient-free temperature profile may be realized using high conductivity materials and thermal system capable of controlling temperatures to the sub-degree level.

5. MIRROR DESIGN AND TESTING

Table 4 lists surface figure requirements for the TMA-63 mirrors. Surface figure requirements are half the optical path difference (OPD). Included are allocations for manufacturing, figuring and mounting. One key element of the test program for SNAP is an end-to-end optical test prior to launch. Vertical or horizontal axis testing are possible, but vertical testing presents advantages from the standpoint of symmetry, and is considered exclusively for this study. Mirrors and support structures sag on length scales significant to the overall alignment and wavefront error budget of TMA-63. Gross mirror displacements may be corrected via motion of the secondary, or by directly offloading the optic. Mirror distortions (sagging) due to gravity must be accounted for in a reduced 1-g test surface figure requirement, or a multi-actuator ground support equipment (GSE) offloading array. When possible through material selection or configuration change, it is preferable to avoid use of an offloading system.

Mirror	Figure error (nm RMS)	Additional figure error during 1-g testing (nm RMS)
Primary (PM)	10	10
Secondary (SM)	7.5	9
Fold (FM)	6	10
Tertiary (TM)	7.5	10

Table 4: Mirror figure requirements, and reduced requirements for 1-g test

A comparative study of various materials and geometries for the four mirrors of TMA-63 was undertaken by Besuner.[17] Materials considered included silicon carbide (SiC), Corning Ultra-Low Expansion glass (ULE™) and Schott Zerodur™. Open, closed and partially closed-back designs with triangular and hexagonal core cutouts were investigated. Designs were rated by thermal stability, strength, dynamics and minimization of figure sag during 1-g optical testing.

	Corning ULE™	Schott Zerodur™ glass	Silicon Carbide	Invar 36	M55J carbon fiber/cyanate ester
Young's modulus (Gpa)	67.6	91.0	310	148	96.5
density (g/cm^3)	2.20	2.53	2.95	8.05	1.9
Stiffness/density ($10^6 m^2/s^2$)	30.1	36.0	105	18.4	50.8
Strength (MPa)	50	70	81	483	690
Coefficient of thermal expansion (CTE) (10^{-6}/K)	0.010-0.015 (various grades)	0.02-0.05 (various grades)	2.4	1.3	-0.07
Conductivity (k) (W/m-K)	1.31	1.46	156	10.2	35
CTE/k (10^{-9} m/W)	7.6-11.5	13.6-34.2	15.4	127	2.0

Table 5: Materials and properties included in TMA-63 trade space

Table 5 lists structural and thermal properties of materials used in the Besuner study. Of the three materials studied, none had a clear advantage in all mirror and loading cases, and each mirror material was selected based on performance and geometrical requirements of the individual mirror. The ratio of stiffness (Young's modulus) to density (included in Table 5) is an important metric in minimizing 1-g sag and maximizing natural frequency. Although promising new techniques for mirror fabrication have been demonstrated,[18] we limit our selections to a conservative set of flight-heritage construction techniques. Partial closed-back designs are manufactured by undercutting a tool-workable material, and produce configuration stiffnesses between open and closed-back designs proportional to the areal coverage of the rear faceplate. Open-back mirrors should have triangular ribs (not hexagonal), in order to preserve continuous load paths across the mirror in the absence of a rear faceplate. Table 6 shows the materials and configurations selected for the room-temperature reference design. It is significant to note that of all the materials, ULE™ has the lowest stiffness to weight ratio; however when manufactured in a closed-back sandwich configuration, its stiffness to weight ratio increases dramatically.

Figure requirements during 1-g testing were met for the SM and TM by material and configuration selection. The PM requires 96 offloaders (vertical test) to reduce gravitationally-induced figure errors to levels below those required for the test. ULE™ and Zerodur™ FM designs required offloading to meet specifications, primarily due to load path disruption by the central hole. A non-offloaded FM design made of SiC is viable. The CTE of SiC is much greater than that of ULE™ or Zerodur™, but because the mirror is flat, bulk temperature changes do not change the radius of curvature. The ratio of CTE to thermal conductivity is similar for SiC, ULE™ and Zerodur™, therefore gradient distortions are comparable for a mirror made of any of the materials.

	Primary	Secondary	Folding Flat	Tertiary
Material	ULE™	ULE™	SiC	ULE™
Outside diameter (mm)	2050	500	720 x 480	730
Inside diameter (mm)	686	N/A	190 x 120	N/A
Radius of curvature of optical surface (mm)	4908	1099	N/A	1406
Shape of front (optic)	Concave	Convex	Flat	Concave
Shape of back	Convex	Flat	Flat, beveled	Flat
Thickness (mm)	200, uniform	100 at center	100, uniform	100 at edge
Construction	Closed-back	Closed-back	Open-back	Closed-back
Cell shape	Honeycomb or triangular	Honeycomb or triangular	Triangular	Honeycomb or triangular
Faceplate bonding	Frit or fusion	Frit or fusion	N/A	Frit or fusion
Mass of mirror (kg)	205	8.9	13.2	18.3
Bipod supports*	3 'normal'	3 'inverted'	3 'inverted'	3 'normal'
First natural frequency on mounts (Hz)	111	85	218	123
Minimum mirror material safety factor	16	40	23	22
Minimum bipod material safety factor	2.7	8	14	4
*'Normal' bipods converge at the mirror; 'inverted' bipods converge at telescope mount end.				

Table 6**:** Mirror configurations considered suitable for SNAP TMA-63.

6. STRAY LIGHT

Stray light requirements for the SNAP observatory are tracked via a systems engineering budget approach. Illuminated objects are analyzed and tracked separately from a tabulation of the solid angles of objects directly and indirectly visible to detector pixels. Stray light sources include foreground Zodiacal light, infrared emissions from warm structures visible to the HgCdTe detectors, starlight diffracted by the secondary mirror and its supports, and moon, Earth and starlight scattered by mirror dust, surface roughness and optical baffles.

Direct solar illumination is the most significant stray light source. The largest element of the observatory, the external baffle, is included primarily to block sunlight, and much less critically, off-axis starlight and stray light produced by occasional illumination of the baffle entrance ellipse by moon and Earthlight. The baffle entrance angle (34˚) was chosen by analyzing worst-case seasonal solar normals experienced at an L2 Lissajous or halo orbit, and extremes of the 15 square degree observation region. Preclusion of all solar and lunar illuminations of the main baffle entrance ellipse would require an unwieldy baffle. Such infrequent lunar and Earth transits are detailed by Jelinsky,[19] and their effects will be minimized by modification of the observation schedule. Sunlight diffracted by the front edge of the baffle is mitigated by a second internal edge, shadowed by the first.

Figure 4 shows the inner baffle and the secondary mirror baffle. (See Figure 4.) The inner baffle, in conjunction with the secondary mirror baffle prevents direct illumination of the fold mirror by off-axis starlight. The inner baffle prevents direct scattering paths from the main baffle to the fold mirror.

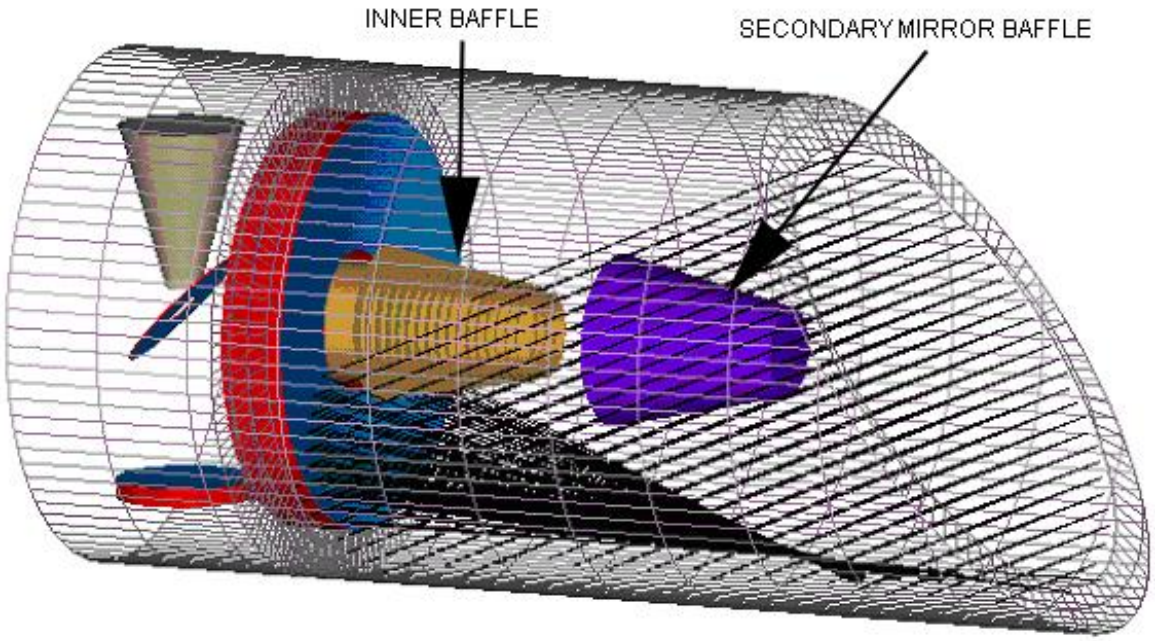

Figure 4: Secondary baffle shadows entrance to inner baffle.

A significant source of stray light results from direct illumination of the focal plane by out-of-field star and Zodiacal light. Glints off the edges of detectors, filter frames and any other structures located above the focal plane can increase the overall stray light level at the detectors. In traditional telescopes, a circular field stop is employed to limit the field of view of the telescope to only that light which contributes signal at the focal plane. The mosaic layout of the SNAP focal plane, and the Cassegrain focus located near the base of the PM lend themselves to installation of a Cassegrain field stop similar in shape to the active detector area on the SNAP focal plane (see Figure 5). The main effect of this baffle is to shadow non-active areas of the focal plane so no light arrives, and adds to the stray light budget.

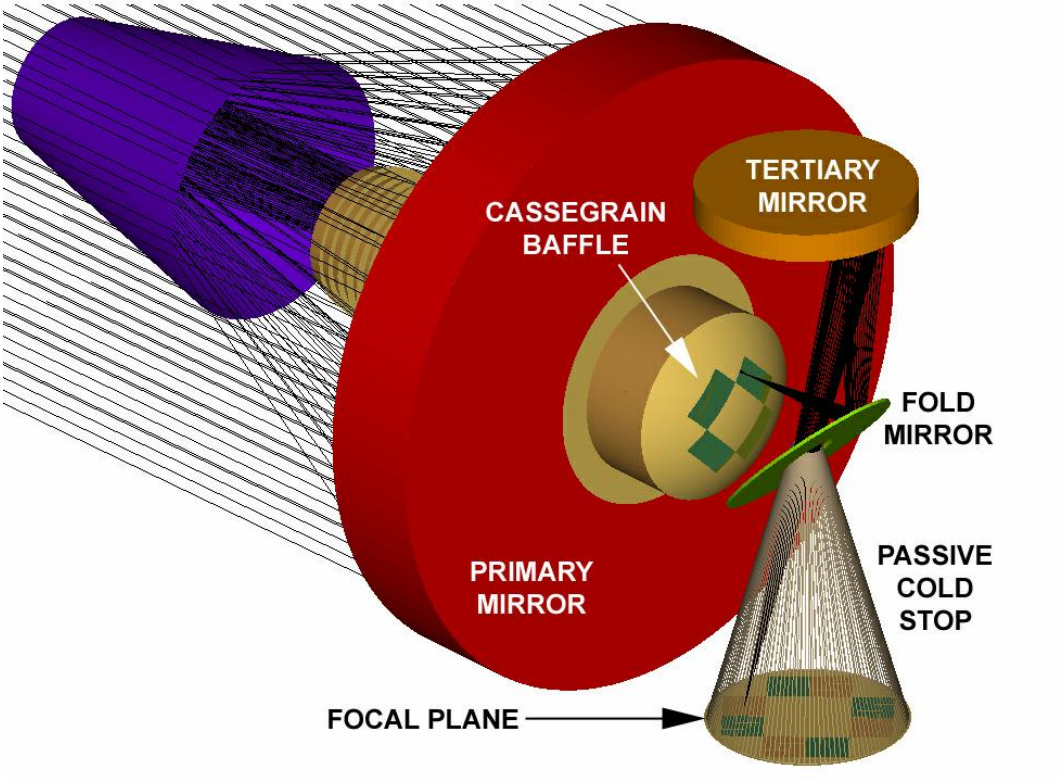

Figure 5: Cutouts in the Cassegrain mask map to images of the detector arrays on the focal plane. This shadows inactive areas of the focal plane, thereby reducing stray light. Additional holes will be placed on the Cassegrain mask to allow light to reach the fine guider chips.

Because the Cassegrain baffle is at a focus, and outside the field of view of the detectors, it does not contribute infrared noise to the detectors. Table 7 lists surfaces visible to pixels on the focal plane, and their subtended angles. Notable in this budget is the 140K passive cold stop, which extends into the hole on the FM, and dominates the solid angle visible to the detector pixels. Although warm surfaces are visible to the pixels (for example the front surface of the Cassegrain baffle is observed after multiple PM/SM reflections), their small solid angles make contributions negligible.

	ε	T(K)	Solid angle (sr)	Photon rate (per second)
Cassegrain	0.02	293	8.36E-05	1.40E-04
Focal Plane	0.87	140	7.61E-05	2.37E-17
Passive Cold Stop	0.87	140	6.28E+00	1.95E-12
Main Baffle	0.87	200	2.85E-04	1.37E-08
Secondary Hat	0.87	200	5.91E-04	2.85E-08
Stovepipe	0.87	220	8.90E-04	2.45E-06
Secondary Struts	0.02	293	1.54E-04	2.57E-04
Deep Space	0.04	293	5.39E-03	1.80E-02

Total Rate	0.01842

Table 7: Detector pixels see primarily the passive cold stop. This table shows the solid angles visible to a detector, the surface temperatures, and an estimate of blackbody emission.

Point source transmittance curve budgeting of the illumination levels of surfaces visible to the detectors is underway. To date, effects including mirror roughness, dust scattering, filter ghosting and reflection and scattering off the main baffle, Cassegrain baffle and cold stop have been quantified and found to be well below Zodiacal levels. This process continues as the observatory matures, and will ultimately produce a comprehensive stray light specification for the SNAP Mission.

8. FUTURE WORK

Optimization of the SNAP mission continues. In particular, optimal sampling for the SNAP measurements, as dictated by the fixed CCD and HgCdTe pixel sizes and the telescope focal length, are the subject of current study. Related studies are underway on dithering strategies for recovery of resolution, and studies of optimal filter bandpasses and shapes.

CONCLUSIONS

The SNAP mission is designed to perform a space-based experiment to study dark energy, and to explore alternate explanations for the universe's expansion acceleration. The baseline three-mirror telescope design meets science requirements, and fits within a launch vehicle fairing. Stray light mitigation strategies, mirror design and test schemes were reported. Detailed engineering design and analysis work has shown that the architecture is mature, and capable of delivering the needed performance using today's technology.

ACKNOWLEDGMENTS

This work was supported by the Director, Office of Science, of the U.S. Department of Energy under Contract No. DE-AC03-76SF00098.

REFERENCES

1. G. Aldering, et al, Supernova/Acceleration Probe: a Satellite Experiment to Study the Nature of the Dark Energy, PASP submitted, 2004.
2. S. Perlmutter et al, Astrophys. J., **517**, p.565, 1999.
3. A.G. Riess et al, Astron. J., **116**, p.1009. 1998.
4. G. Aldering et al, Proc. SPIE **4835** #21, 2002.
5. A. Kim et al, Proc. SPIE **4836** #10, 2002.
6. Various authors, Session 97 "Probing Dark Energy with SNAP" and Session 126 "SNAP", 201st Meeting of the AAS, Seattle, Jan 2003.
7. M. Lampton et al, Proc. SPIE **4849** pp.215-226, 2002.
8. M. Lampton et al, Proc. SPIE **4854**, 2002.
9. M. Lampton et al, Proc. SPIE **5166**, 2003.
10. C.Bebek et al, Proc. SPIE 5164 #10, 2003.
11. A. Ealet et al, Proc. SPIE **4850** #165, 2002.
12. P. Jelinsky, SNAP L2 Orbit Eclipse/Antenna Study, Internal SNAP Technical Memorandum, 2004 (http://snap.lbl.gov/bscw/bscw.cgi/d85886/SNAP-TECH-04001.doc).
13. D. Korsch, Appl.Optics **11,** p.2986, 1972; **16**, p.2074, 1977; **19**, p.3640, 1980.
14. M. Lampton, Computers in Physics, Vol. 11, No. 1, 1997.
15. M. Born and E. Wolf, *Principles of Optics* (Pergamon, Oxford, 1980), Chapter IX, p. 464.
16. M. Sholl, SNAP Optomechanical Tolerances, Internal SNAP Technical Memorandum, 2003.
17. R. Besuner, SNAP Telescope Mirrors, Internal SNAP Technical Memorandum, 2004.
18. L. Matson, D. Mollenhauer, Advanced Materials and Processes for Large, Lightweight, Space-Based Mirrors, Air Force Research Laboratory, 2003.
19. P. Jelinsky, SNAP L2 Orbit Scattering Angles for near Ecliptic Pole Pointings, Internal SNAP Technical Memorandum, 2004 (http://snap.lbl.gov/bscw/bscw.cgi/d85889/SNAP-TECH-04002.doc).